Journal of Solid State Chemistry **148,** 20–25 (1999)
Article ID jssc.1999.8291, available online at http://www.idealibrary.com on IDEAL®

Cation Size Variance Effects in High-Tolerance Factor $Ln_{0.7}M_{0.3}MnO_3$ Perovskites

Lide M. Rodríguez-Martínez, Helmut Ehrenberg, and J. Paul Attfield[1]

Department of Chemistry, University of Cambridge, Lensfield Road, Cambridge CB2 IEW, United Kingdom; and Interdisciplinary Research Centre in Superconductivity, University of Cambridge, Madingley Road, Cambridge CB3 0HE, United Kingdom

Received January 12, 1999; accepted March 23, 1999

A series of five $Ln_{0.7}M_{0.3}MnO_3$ perovskites (Ln = trivalent lanthanide; M = divalent alkaline earth) has been prepared. These have the same mean A-cation site radius of 1.26 Å (equivalent to a perovskite tolerance factor of 0.98) but varying amounts of A-cation size disparity quantified by the size variance σ^2. As this increases, the temperatures of the metal–insulator and Curie transitions show a strong linear decrease but that of the structural transition between rhombohedral $R\bar{3}c$ and orthorhombic *Imma* phases increases. Extrapolation from these and previous data indicates that the maximum metal–insulator temperature for an $Ln_{0.7}M_{0.3}MnO_3$ perovskite is ~ 550 K. Different methods for estimating the Curie temperature are compared. © 1999 Academic Press

INTRODUCTION

The complex electronic and magnetic properties observed in doped manganese oxide perovskites of the general formula $Ln_{1-x}M_xMnO_3$ (Ln = trivalent lanthanide, M = divalent alkaline earth cation) have attracted considerable interest in recent years (1, 2). Over certain ranges of composition, these materials exhibit a paramagnetic insulator to ferromagnetic metal transition as the temperature decreases, characterised by a maximum in the electrical resistivity, ρ_m, at a temperature, T_m, which is close to the Curie temperature T_C. When a magnetic field is applied, the resistivity decreases and shifts to higher temperatures, producing colossal magnetoresistances around T_m (3, 4). This phenomenon was initially explained in terms of a double-exchange mechanism (5, 6), in which localized t_{2g}^3 states on adjacent Mn ions interact via itinerant e_g electrons due to the mixed Mn^{3+}/Mn^{4+} valence states. However, this mechanism is insufficient to account for the metal–insulator transition in these perovskites, and the additional presence of electron-localizing (polaron) effects due to John Teller distortions of the $Mn^{III}O_6$ octahedra appears to play an important role (7, 8).

The magnetotransport properties of these materials have been found to be dependent on external pressure (9, 10), applied magnetic field (11, 12), temperature (13), the chemical composition (9, 14–16). The latter includes the effects of doping (Mn oxidation state) (15, 17) the average size of the A-site (Ln^{3+} and M^{2+}) cations, $\langle r_A \rangle$ (16, 18), and the effect of cation size disparity (19). The latter is quantified by the variance of the A-cation radius distribution, $\sigma^2 = \langle r_A^2 \rangle - \langle r_A \rangle^2$, where r_A are standard 9-coordinate ionic radii (20) with values ranging from 1.216 to 1.132 Å for Ln = La, Sm and 1.18, 1.31, and 1.47 Å for M = Ca, Sr, Ba, respectively. It was previously shown that in a series of $Ln_{0.7}M_{0.3}MnO_3$ perovskites with constant $\langle r_A \rangle = 1.23$ Å, the transition temperature T_m decreases linearly with σ^2 (19). This effect, attributed to random displacements of the oxygen atoms due to A-site disorder, shows the strong influence of local, incoherent lattice strains on the metal–insulator transition in manganese perovskites (21, 22). In this paper, we compare the previous results with those corresponding to a new series of $Ln_{0.7}M_{0.3}MnO_3$ perovskites with variable σ^2 and a larger average radius $\langle r_A \rangle = 1.26$ Å. This is equivalent to a perovskite tolerance factor of 0.98, allowing for the scaling between the 9-coordinate radii used and the 12-coordination of A cations in the ideal perovskite structure.

EXPERIMENTAL

Polycrystalline $Ln_{0.7}M_{0.3}MnO_3$ perovskite oxides were prepared under identical conditions by a solid state reaction of appropriate mixtures of oxides (La_2O_3, Pr_6O_{11}, Nd_2O_3, BaO_2, and MnO_2) and carbonates ($SrCO_3$ and $CaCO_3$) in air at 950°C for 16 h. The preheated powders were ground, pressed into pellets, sintered at 1350°C for 24 h, and quenched to room temperature. The mean oxidation state of manganese was determined by iodometric titration. The samples were characterized by X-ray powder diffraction at

[1]To whom correspondence should be addressed. E-mail: jpa14@cam.ac.uk. Fax: + 44 1223 336362.

0022-4596/99 $30.00

room temperature using a STOE/STADI-P powder diffractometer with Ge(111) monochromatized Cu$K\alpha_1$ radiation. The diffraction patterns were Rietveld fitted using the GSAS program (23).

Electrical resistivity measurements on sintered polycrystalline bars (approximate dimensions $1.5 \times 2 \times 8\ mm^3$) were performed between 100 and 400 K by a conventional four-probe method. Magnetizations of powdered samples were recorded with a SQUID magnetometer (MPMS 2, Quantum Design) as a function of temperature, $M(T)$, under a magnetic field of 500 G on field-cooled samples, and as a function of magnetic field, $M(H)$, at several temperatures.

RESULTS

The Mn oxidation states obtained by iodometric titration (Table 1) show that the $Ln_{0.7}M_{0.3}MnO_3$ compositions are very close to being oxygen stoichiometric with no dependence of the oxygen content upon σ^2. Powder X-ray patterns revealed single-phase perovskites with rhombohedral $R\bar{3}c$ symmetry for the first three samples and an orthorhombic ($\sqrt{2} \times 2 \times \sqrt{2}$) superstructure for the two highest σ^2 samples (Fig. 1). No evidence for the coexistence of these different structural phases is observed by laboratory X-ray powder diffraction (Fig. 2). Both *Pnma* and *Imma* orthorhombic superstructures are known for $Ln_{0.7}M_{0.3}MnO_3$ perovskites. These two symmetries cannot be distinguished on the basis of the present X-ray powder patterns, but materials with large $\langle r_A \rangle$ values are known to adopt *Imma* symmetry (24, 25), as confirmed by a recent neutron powder diffraction study of $Nd_{0.7}Ba_{0.3}MnO_3$ (26) which has $\langle r_A \rangle = 1.255$ Å and $\sigma^2 = 0.0198$ Å^2, close to the high σ^2 end of our $\langle r_A \rangle = 1.26$ Å series. These orthorhombic samples were therefore assumed to have *Imma* symmetry in the Rietveld fits which gave R_{wp} residuals of 2.7–4.0% for the five refinements. The results of the refinements, titrations, and physical measurements are reported in Table 1.

Resistivity measurements (Fig. 3) show insulator-to-metal transitions in all the samples. ρ_m increases and T_m decreases as σ^2 increases (Table 1). Some of these compositions show the presence of a shoulder at lower temperatures which has been previously observed in other samples with a high cation size mismatch (19, 25). Corresponding features are not seen in the magnetization data for these samples.

The insulator–metal transition temperature, T_m, appears very close to the Curie temperature, T_C, which also shows a strong dependence on σ^2. Sharp ferromagnetic transitions are observed for compositions with low σ^2, but for those with large values of σ^2 the transitions are much broader. This behavioral change coincides with the structural transition at $\sigma^2 \approx 0.011$ Å^2. To quantify the dependence on σ^2, values of T_C were determined by three commonly used methods. T_{C1} was found from the minimum in $d(M/H)/dT$ (16), and a tangent to the $M(T)$ curve at this point was extrapolated to $M = 0$, giving the second estimate T_{C2} (as shown in Fig. 4). In addition, variable field scans at several temperatures below T_C were used to determine the spontaneous magnetizations by extrapolating the high-field slopes to $H = 0$. In the mean field approximation, the temperature dependence of the spontaneous magnetization $M(T)$ is given by the self-consistent solution of

$$M(T)/M_0 = B_S[3(M(T)/M_0)(S/(S+1)(T_C/T)], \quad [1]$$

where B_S is the Brillouin function for spin $S = 3/2$. The third estimate T_{C3} and the saturation magnetization at zero temperature, M_0, were obtained from fits of Eq. (1) to the spontaneous magnetization data (Fig. 5). The M_0 values

TABLE 1
Chemical, Structural, and Physical Data for Five $Ln_{0.7}M_{0.3}MnO_3$ Perovskites with $\langle r_A \rangle = 1.26$ Å

A-site: $Ln_{0.7}$	$La_{0.62}Pr_{0.08}$	$La_{0.57}Nd_{0.13}$	$La_{0.70}$	$La_{0.27}Pr_{0.43}$	$La_{0.48}Nd_{0.22}$
$M_{0.3}$	$Sr_{0.18}Ba_{0.12}$	$Ba_{0.14}Sr_{0.16}$	$Ca_{0.11}Ba_{0.19}$	$Sr_{0.10}Ba_{0.20}$	$Ba_{0.23}Ca_{0.07}$
σ^2 (Å^2)	0.0075	0.0089	0.0104	0.0124	0.0136
Mn oxidation state	3.30(6)	3.32(4)	3.34(2)	3.26(4)	3.30(2)
Space group	$R\bar{3}c$	$R\bar{3}c$	$R\bar{3}c$	*Imma*	*Imma*
a (Å)	5.5196(1)	5.5195(1)	5.5228(1)	5.4940(1)	5.4979(1)
b (Å)				7.7621(2)	7.7688(2)
c (Å)	13.4107(2)	13.4114(2)	13.4256(3)	5.5319(1)	5.5324(1)
V/Z (Å^3/f.u.)	58.972(2)	58.973(2)	59.106(2)	58.977(3)	59.075(3)
ρ_m (Ω-cm)	0.159	0.257	0.744	1.00	1.96
T_m(K)	354	337	313	269	252
T_{C1} (K)	336	328	305	260	243
T_{C2} (K)	348	338	318	292	283
T_{C3} (K)	365	348	332	282	277
μ_0 (μ_B)	3.74	3.71	3.70	3.63	3.69

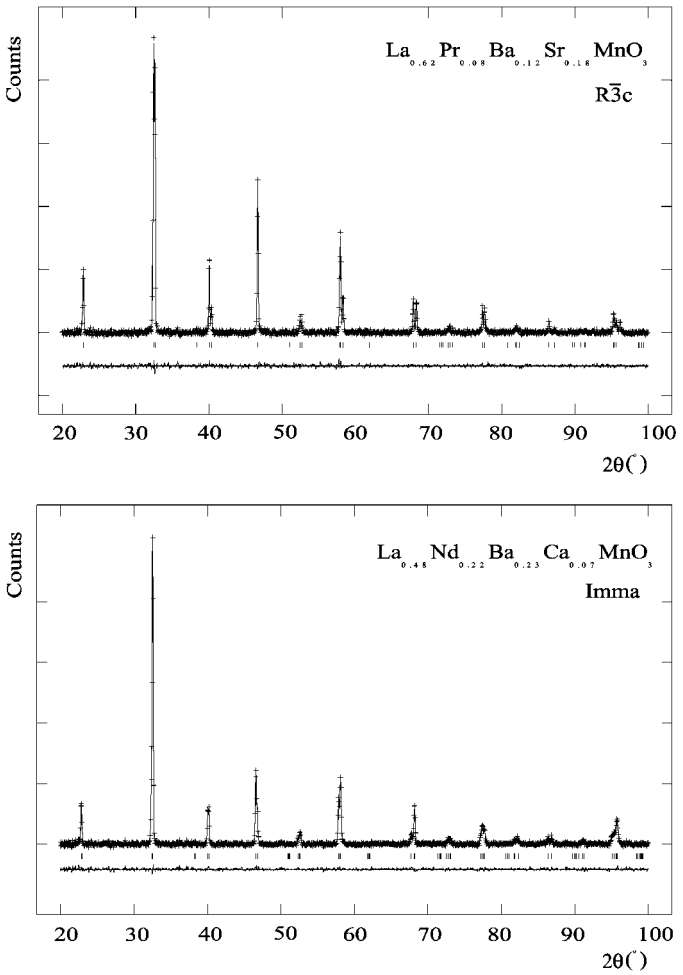

FIG. 1. Observed and calculated power X-ray diffraction data for two of the $\langle r_A \rangle = 1.26$ Å manganites showing typical rhombohedral and orthorhombic symmetries.

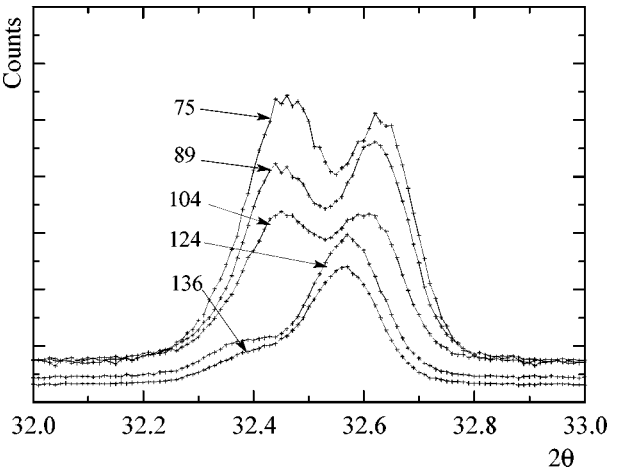

FIG. 2. The evolution of the splitting of the (110) X-ray diffraction peak (indexed on the ideal cubic cell) as the symmetry changes from rhombohedral to orthorhombic, with σ^2 values ($\times 10^4$ Å^2) labeled.

give saturation magnetic moments per Mn ion, μ_0, close to the theoretical value of 3.7 μ_B. These magnetic results are shown in Table 1 and the T_m's and three sets of T_C's are plotted in Fig. 6. Fits of the linear equation

$$T_X = T_X^0 - p_1\sigma^2 \qquad [2]$$

to each transition give the parameters in Table 2.

DISCUSSION

The five samples in this series of $\langle r_A \rangle = 1.26$ Å $Ln_{0.7}M_{0.3}MnO_3$ perovskites are all homogenous and have the same Mn doping level within error. Differences in lattice and physical properties result from the systematic increase in the A-cation size mismatch which is quantified by the size variance σ^2. The cell volume per perovskite unit (V/Z in Table 1) does not change significantly with σ^2, as might be expected for samples with a fixed $\langle r_A \rangle$ and doping level. However, the cell parameters and symmetry do change, most notably from rhombohedral $R\bar{3}c$ to orthorhombic *Imma* superstructures with increasing σ^2. The former is known to be the high-temperature phase (18), and so we conclude that the structural transition temperature changes from < 300 K for $\sigma^2 < 0.011$ Å^2 to > 300 K above this value. Previous studies (21, 22) have shown that the $R\bar{3}c$–*Pnma* transition in $Ln_{0.7}M_{0.3}MnO_3$ perovskites with a smaller $\langle r_A \rangle = 1.23$ Å is also strongly σ^2 dependent, as is the tetragonal–orthorhombic structural transition in $Ln_{1.85}M_{0.15}CuO_4$ superconductors (27). $dT_X/d\sigma^2$ is large and positive ($\sim 50{,}000$ KÅ^{-2}) for these structural transitions, but negative and with smaller magnitudes (1,000–30,000 KÅ^{-2}) for the electronic and magnetic transitions (28).

The ferromagnetic metal-to-paramagnetic insulator transition is observed to be very sensitive to σ^2, as found

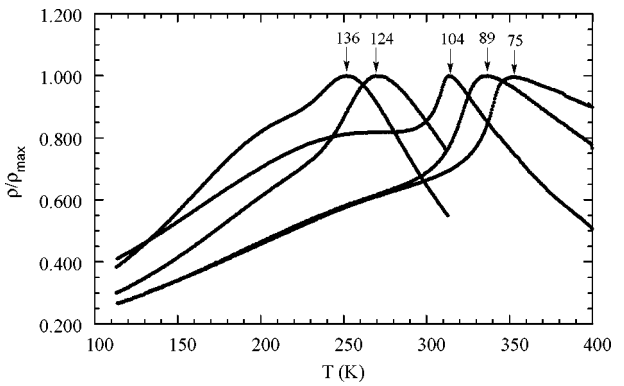

FIG. 3. Resistivity measurements for the $\langle r_A \rangle = 1.26$ Å manganite series with σ^2 values ($\times 10^4$ Å^2) labeled.

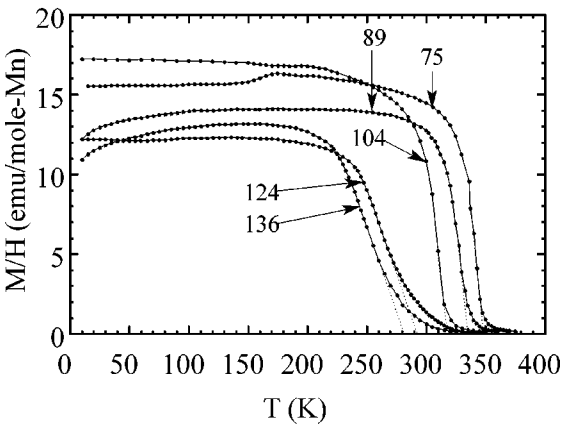

FIG. 4. Magnetization/field measurements for the $\langle r_A \rangle = 1.26$ Å manganite series with σ^2 values ($\times 10^4$ Å^2) labeled ($H = 0.05$ T).

in the previous $\langle r_A \rangle = 1.23$ Å series and decreases by $\sim$100 K over the experimental σ^2 range. No discontinuity in physical properties is observed at the rhombohedral–orthorhombic transition, except for a broadening of the magnetic transition in low fields, but a study of further samples on either side of the transition will be needed to confirm this. To quantify the σ^2 dependence of the transition, several estimates of the temperature can be made experimentally as described above. These all show essentially linear decreases with σ^2, and the errors in the fitting parameters (Table 2) reflect the random deviations from linearity. The metal–insulator transition temperature, T_m, obtained from the resistivity maximum shows a good linear correlation with σ^2. The slope $p_1 = -dT_m/d\sigma^2$ is significantly less than the value of 20,600 KÅ^{-2} found in the $\langle r_A \rangle = 1.23$ Å series and the intercept T_m^0 is greater than the

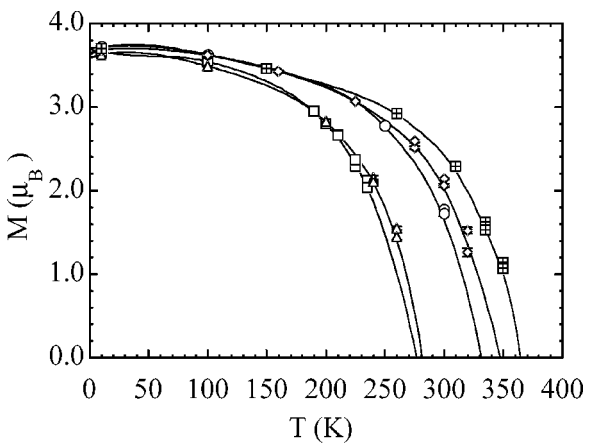

FIG. 5. Spontaneous magnetization data for the five samples (with σ^2 increasing in the following order: crossed squares, diamonds, circles, triangles, and open squares) showing fits of Eq. [1].

previous 400 K value (19), showing the systematic dependence of these parameters upon $\langle r_A \rangle$.

The T_{C1} estimate from the minimum in $d(M/H)/dT$ is not a correct definition of the Curie temperature; however, the values correlate strongly with the T_m data, being $\sim$10 K less throughout. The T_{C3} values obtained from fits to the spontaneous magnetization data also correlate strongly with the T_m values, but are systematically greater by $\sim$15 K. Despie this, the T_X^0 and p_1 parameters obtained from the T_{C1} and T_{C3} data are within error of those from T_m. T_{C2} values were obtained by extrapolating the maximum slope in the low-field $M(T)$ curves to $M = 0$. Although this is a thermodynamically correct definition of T_C in an applied field, and the data give an excellent linear correlation with σ^2, the slope and intercept are significantly different to those obtained by the other three methods. This demonstrates that the latter method of estimating T_C is less useful for polycrystalline manganites, perhaps due to domain effects at low-field strengths.

T_m^0 is an experimental estimate of the metal–insulator transition temperature at zero A-cation size variance for a given mean radius $\langle r_A \rangle$. T_m^0 increases up to a maximum value, T_m^*, when $\langle r_A \rangle$ has the ideal value r_A^0, giving a perovskite tolerance factor of 1.0. $Ln_{0.7}M_{0.3}MnO_3$ perovskites have $r_A^0 = 1.30$ Å. It has previously been suggested (19) that T_m^0 should vary as

$$T_m^0 = T_m^* - p_2(r_A^0 - \langle r_A \rangle)^2 \qquad [3]$$

by analogy with Eq. [2]. (An equivalent argument is that σ^2 and $(r_A^0 - \langle r_A \rangle)^2$ are respectively the incoherent and coherent parts of $\langle (r_A^0 - r_A)^2 \rangle$ which is a measure of the total strain on the MnO_3 network due to the A-site cations (29).) T_m^* was previously estimated by assuming that p_1 is constant, but the results in this paper show that this is not the case, as suggested by Damay *et al.* (30). To avoid this problem, Fig. 7 shows a plot of T_m^0 vs $(r_A^0 - \langle r_A \rangle)^2$ using the extrapolated T_m^0 values from the $\langle r_A \rangle = 1.23$ and 1.26 Å series plus reported T_m's for six samples with smaller $\langle r_A \rangle$'s and very little disorder ($\sigma^2 < 0.0005$ Å^2) (these

TABLE 2
Fitted Parameters Using Eq. [2] to Describe the Dependence of the Metal–Insulator Transition and Three Estimates of the Curie Temperature, As Described in the Text

Transition	T_X^0 (K)	p_1 (KÅ^{-2})
T_m	489(11)	17,400(1000)
T_{C1}	470(18)	16,300(1600)
T_{C2}	435(7)	11,300(600)
T_{C3}	486(18)	15,600(1700)

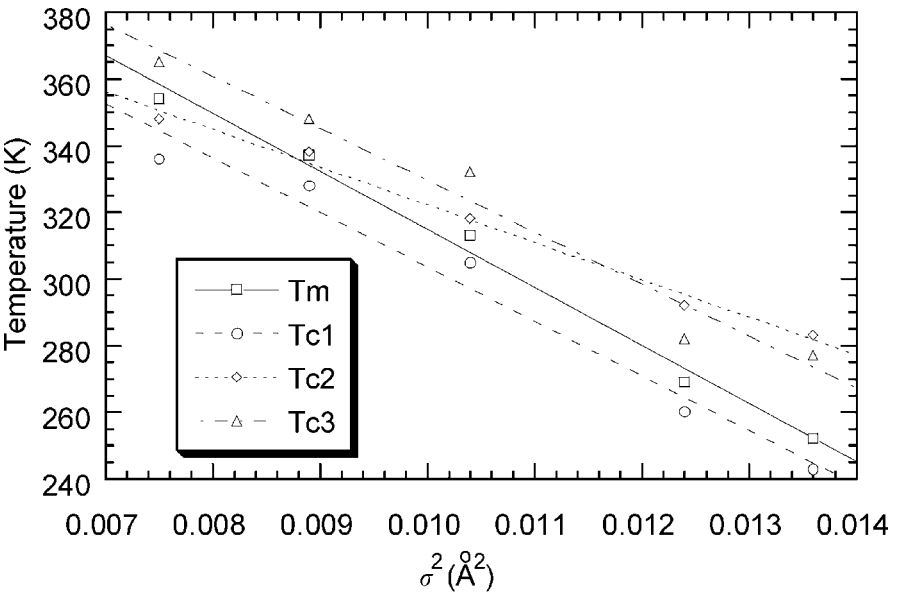

FIG. 6. Plots of the metal–insulator transition temperature T_m and the three estimates of T_C vs σ^2 with linear fits shown.

are $(La_{0.7-y}Pr_yCa_{0.3})MnO_3$ ($y = 0$, 0.175, 0.35, 0.525, 0.6) (16) and $(La_{0.69}Y_{0.01}Ca_{0.3})MnO_3$ (29)). The variation is linear with fitted parameters $T_m^* = 555(11)$ K and $p_2 = 33{,}700(1100)$ KÅ^{-2}, little different from those reported previously. Hence, the maximum metal–insulator transition temperature that is physically possible in a 30% doped manganite perovskite is ≈ 550 K, although the combination of *A*-cation size and mismatch effects reduces observable values to < 360 K for the available *Ln* and *M* cations.

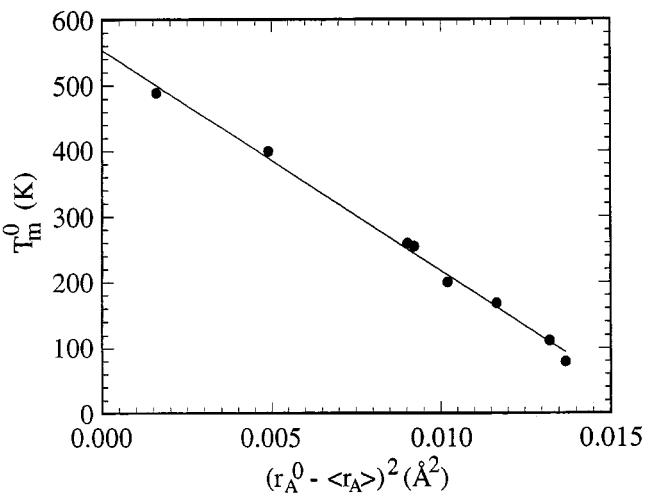

FIG. 7. Plot of zero variance T_m^0 for $Ln_{0.7}M_{0.3}MnO_3$ perovskites against $(r_A^0 - \langle r_A \rangle)^2$ showing the linear fit of Eq. (3).

ACKNOWLEDGMENTS

We thank the Basque Government for a studentship for L.M.R.M. and the EU for a TMR fellowship for H.E.

REFERENCES

1. C. N. R. Rao, A. K. Cheetham, and R. Mahesh, *Chem. Mater.* **8,** 2421 (1996).
2. C. N. R. Rao and A. Arulraj, *Curr. Opin. Solid State Mater. Sci.* **3,** 23 (1998).
3. R. von Helmolt, J. Wecker, B. Holzapfel, L. Schultz, and K. Samwer, *Phys. Rev. Lett.* **71,** 2331 (1993).
4. R. M. Kusters, J. Singleton, D. A. Keen, R. McGreevy, and W. Hayes, *Physica B* **155,** 362 (1989).
5. C. Zener, *Phys. Rev.* **82,** 403 (1951).
6. P. G. de Gennes, *Phys. Rev.* **118,** 141 (1960).
7. A. J. Millis, P. B. Littlewood, and B. I. Shraiman, *Phys. Rev. Lett.* **74,** 5144 (1995).
8. A. J. Millis, B. I. Shraiman, and R. Mueller, *Phys. Rev. Lett.* **77,** 175 (1996).
9. H. Y. Hwang, T. T. M. Palstra, S.-W. Cheong, and B. Batlogg, *Phys. Rev. B.* **52,** 15046 (1995).
10. J. J. Neumeier, M. F. Wundley, J. D. Thompson, and R. H. Heffner, *Phys. Rev. B.* **52,** R7006 (1995).
11. A. Asamitsu, Y. Moritomo, Y. Tomioka, T. Arima, and Y. Tokura, *Nature* **373,** 407 (1995).
12. H. Kuwahara, Y. Tomioka, A. Asamitsu, Y. Moritomo, and Y. Tokura, *Science* **270,** 961 (1995).
13. Y. Tokura, A. Urushibara, Y. Moritomo, T. Arima, A. Asamitsu, G. Kido, and N. Furukawa, *J. Phys. Soc. Jpn.* **63,** 3931 (1994).
14. R. Mahesh, R. Mahendiran, A. K. Raychaudhuri, and C. N. R. Rao, *J. Solid State Chem.* **120,** 204 (1995).
15. P. Schiffer, A. P. Ramirez, W. Bao, and S.-W. Cheong, *Phys. Rev. Lett.* **75,** 3336 (1995).

16. H. Y. Hwang, S.-W. Cheong, P. G. Radaelli, M. Marezio, and B. Batlogg, *Phys. Rev. Lett*. **75,** 914 (1995).
17. R. Mahesh, R. Mahendiran, A. K. Raychaudhuri, and C. N. R. Rao, *J. Solid State Chem.* **114,** 297 (1995).
18. P. G. Radaelli, M. Marezio, H. Y. Hwang, and S.-W. Cheong, *J. Solid State Chem.* **122,** 444 (1996).
19. L. M. Rodriguez-Martinez and J. P. Attfield, *Phys. Rev. B*. **54,** R15622 (1996).
20. R. D. Shannon, *Acta Crystallogr. A* **32,** 751 (1976).
21. L. M. Rodriguez-Martinez and J. P. Attfield, *Phys. Rev. B*. **58,** 2426 (1998).
22. L. M. Rodriguez-Martinez and J. P. Attfield, *Chem. Mater*., in press.
23. A. C. Larson and R. B. von Dreele, "GSAS: General Structure Analysis System," LANSCE, MS-H805, Los Alamos National Laboratory, Los Alamos, NM, 1994.
24. Z. Jirak, E. Pollert, A. F. Andersen, J. C. Grenier, and P. Hagenmuller, *Eur. J. Solid State Inorg. Chem.* **27,** 421 (1990).
25. A. Barnabe, F. Millange, A. Maignan, M. Hervieu, B. Raveau, G. van Tendeloo, and P. Laffez, *Chem. Mater*. **10,** 252 (1998).
26. F. Millange, Ph.D. thesis, University of Caen, France, 1998.
27. J. P. Attfield, A. L. Kharlanov, and J. A. McAllister, *Nature* **394,** 157 (1998).
28. J. P. Attfield, A. L. Kharlanov, J. A. McAllister, and L. M. Rodriguez-Martinez, "Proceedings of the Materials Research Society," 1998 Fall Meeting, in press.
29. J. P. Attfield, *Chem. Mater*. **10,** 3239 (1998).
30. F. Damay, C. Martin, A. Maignan, and B. Raveau, *J. Appl. Phys.* **82,** 6181 (1997).
31. A. Maignan, Ch. Simon, V. Caignaert, and B. Raveau, *J. Appl. Phys.* **79,** 7891 (1996).